INSTITUTE OF PHYSICS PUBLISHING JOURNAL OF PHYSICS D: APPLIED PHYSICS

J. Phys. D: Appl. Phys. **38** (2005) 3403–3411 doi:10.1088/0022-3727/38/18/013

Onset voltage of negative corona on dielectric-coated electrodes in air

Mahmoud Mohamed El-Bahy and Mohamed Anwar Abou El-Ata

Faculty of Engineering at Shubra, Electrical Engineering Department, Zagazig University-Benha Branch, 108 Shubra Street, Cairo, Egypt

Received 21 February 2005, in final form 27 July 2005
Published 2 September 2005
Online at stacks.iop.org/JPhysD/38/3403

Abstract

This paper describes theoretical and experimental investigations of the effect of an electrode coating on the onset voltage of a corona on negatively stressed electrodes. Dielectric-coated hemispherically-capped rod-to-plane gaps positioned in air are investigated. The onset voltage is calculated based on the self-recurring single electron avalanche developed in the investigated gap. Accurate calculation of the electric field in the vicinity of a coated rod and its correlation to the field values near a bare rod of the same radius are obtained using the charge simulation method. The calculated field values are utilized in evaluating the onset voltage of the corona. Also, laboratory measurements of the onset voltage on bare and coated electrodes are carried out. The effects of varying the field nonuniformity, the coating thickness and its permittivity on the onset voltage values are investigated. The results show that coating the electrodes with a dielectric material is effective in increasing the onset voltage of the corona on its surface. The calculated onset voltage values for coated and bare electrodes agree satisfactorily with those measured experimentally.

1. Introduction

Gas-insulated substations (GIS) are successfully used for high-voltage ac power systems. With the tremendous increase in power transmitted over distances greater than 500 miles [1], dc transmission has become competitive, and many dc transmission lines are installed all over the world. This has created a growing interest in the study of self-maintained corona discharges on dc transmission lines. The problems associated with the corona discharge are power loss, audible noise and radio and TV interference [2]. Also, the corona discharge is important in practical high-voltage insulation systems because it can lead to deterioration of the insulating qualities of the gas as well as to production of toxic or corrosive by-products [3, 4].

Insulation systems are typically designed to minimize corona discharges. For any set of electrodes, the onset voltage of the corona is an important design consideration since a corona can limit the performance of any given configuration of electrical conductors [5]. So, it should be ensured that this voltage is higher than the rated operating voltage of the equipment. Hence, knowledge of this voltage is of paramount importance in gas-insulated systems. Also, measurement of this voltage provides an indication of the dielectric strength of the air, since the basic theory used to predict this voltage in nonuniform fields is the same as that which applies to uniform field breakdown [6]. The extent to which one can limit the corona discharge depends on one's ability to understand the basic mechanisms that can influence the initiation and development of the discharge.

A dielectric coating material on a stressed electrode may lead to an acceptable solution for minimizing the corona discharge; i.e. it increases the onset voltage of a corona on its surface [7]. The insulation performance of gas-gaps is improved by using dielectric-coated electrodes [8–10]. Tests have shown that an electrode having a thick insulating layer is less noisy than the bare electrode [11]. More research in this area is of great importance since the improvements obtained so far in insulation ability are substantial and remarkable [7, 9, 10]. Coating electrodes reduces the degree of surface roughness, thus decreasing high local electric fields. Electrodes in GIS may be coated with a dielectric material to restore some of the dielectric strength of the compressed gas that is lost due to surface roughness and contamination with conducting particles [12, 13]. This will encourage high-voltage engineers to construct extra-high-voltage systems.

This paper aims to investigate the effect of a surface coating on the onset voltage of a disruptive corona on a

hemispherically-capped rod electrode stressed by a negative dc voltage, while the opposite electrode is considered as a grounded plane. At the initiation of the disruptive corona phenomenon (in a nonuniform field), a hissing noise is heard and ozone gas is formed [14]. The onset voltage is calculated based on the self-recurring single electron avalanche developed in the investigated gap. This calls first for accurate calculation of the electric field in the vicinity of the coated electrode and its correlation to the field values near a bare electrode of the same radius. The electric field calculation is based on the accurate charge simulation method (CSM) [6, 7, 15] using discrete charges for electrode and dielectric simulation. The calculated field values are utilized for evaluating the onset voltages for both coated and bare electrodes. To check the accuracy of the proposed theoretical model, laboratory measurements are carried out. As is well known for rod–plane gaps [16, 17], the onset voltage of the corona is usually the lowest when the rod electrode is stressed negatively. This is why this paper is aimed at presenting the onset voltage of a corona when a negative dc voltage stresses the coated rod electrode.

2. Method of analysis

2.1. Electric field calculation

The analysis is based on the CSM. The attractiveness of the technique, when compared with the finite-element and finite difference methods, emanates from its simplicity in representing the equipotential surfaces of the electrodes, its application to unbounded arrangements whose boundaries extend to infinity and its direct determination of the electric field [6].

In the CSM [6, 15], the distributed charges on the surface of the stressed electrode(s) are replaced by a set of fictitious simulation charges arranged inside the electrode, i.e. outside the space in which the electric field is to be computed. However, the surface charge on the interface between two dielectrics is simulated by two sets of charges on both sides of the dielectric interface. Satisfaction of the pertinent boundary conditions, namely, the Dirichlet condition at the stressed electrode(s) and the Neumann condition at the dielectric interface(s), results in a set of equations whose simultaneous solution determines the unknown simulation charges [7, 15]. Knowing the simulation charges, the electric potential and field can be calculated at any point in the arrangement investigated.

2.1.1. Simulation of charge on coated electrode. Figure 1 shows a coated hemispherically-capped rod-to-plate electrode system stressed by a voltage V and positioned in air. The stressed electrode is coated with a dielectric layer of thickness t and relative permittivity ε_r. It has a radius R and is located at a height H above the ground plane, which is assumed to be infinitely large.

The distributed charge on the stressed electrode surface is simulated by two sets of charges arranged inside the electrode (figure 1). The first set simulates the hemispherical rod tip. A single point charge is located at the centre of the rod tip, and a number of ring charges (n_e) are distributed uniformly in the angular direction inside the hemispherical tip. The radius

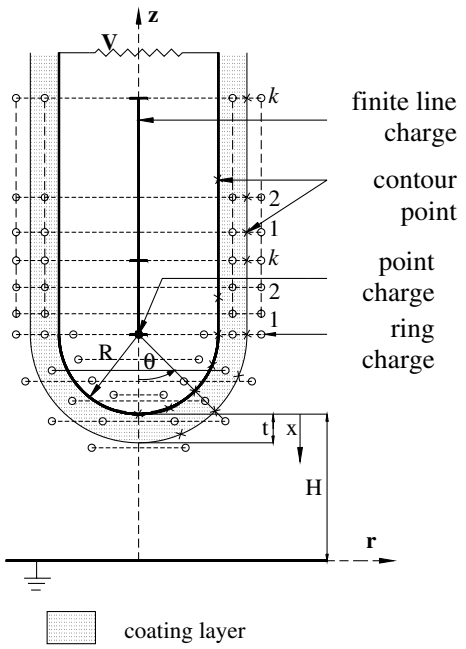

Figure 1. Discrete simulation charges and boundary points for dielectric-coated hemispherically-capped rod-to-plane gap.

of each ring envelope is a fraction, f_0, of the tip radius, R (figure 1). The second set simulating the cylindrical part of the rod is a set of m_e finite line charges extended along the rod axis in cascade. The length of the line charges increases successively. The first line starts at the tip centre with a length, l, of f_1 times the rod radius. Hence, the length $l(i)$ of the ith line charge is $f_2^{(i-1)}$ times the preceding one, $f_2^{(i-1)} > 1$; i.e.

$$l(i) = f_2^{(i-1)} f_1 R, \qquad i = 1, 2, \ldots, m_e. \tag{1}$$

Hence, the number of distributed charges on the stressed electrode surface, N_e, equals $(1 + n_e + m_e)$.

In the dielectric coating layer, the dipoles are aligned by the electric field, resulting from the voltage, V, applied to the stressed electrode, and compensate each other through the volume of the coating layer, leaving net charges at the interface between the coating layer and the surrounding air [6, 15]. These surface charges are simulated by two sets of ring charges. Each set is located at an envelope, one placed inside the dielectric coating layer having a number N_d, and the other placed in the surrounding air having a number N_a. The two sets of ring charges are located at equal distances (δt) from the coating surface. Then, the radii of the two sets of the ring charges envelopes are given as $(R + t - \delta t)$ and $(R + t + \delta t)$ inside the coating layer and outside it in the surrounding air, respectively.

The hemispherical portion of the coating layer is simulated by ring charges having numbers n_d and n_a inside and outside the coating layer, respectively, $n_d = n_a$. These charges are distributed uniformly in the angular direction inside the hemispherical portion. Also, the cylindrical portion of the coating layer is simulated by two groups of ring charges: one is inside the layer having charges of number m_d and the other is outside it in the air having charges of number m_a, $m_d = m_a$.

Corresponding to each finite line charge simulating the rod, k ring charges are selected inside and outside the dielectric. Thus, the number m_d equals km_e. Therefore, the density of the ring charges is decreasing along the z-axis. Hence, at the coating surface the first set of simulation ring charges inside the coating layer has a number $N_d = n_d + m_d$ and the second set outside it has a number $N_a = n_a + m_a$, where $N_d = N_a$. Subsequently, the number of simulation charges for the coated hemispherically-capped rod as a whole equals N; $N = N_e + N_d + N_a$. To maintain the ground plane at zero potential, images of the simulation charges are considered.

2.1.2. Determination of the unknown simulation charges. In order to determine the magnitude of the simulation charges, a set of boundary points on the electrode surface is chosen with their number, N_e, equal to that of the simulation charges inside the electrode, and another set of boundary points at the interface between the coating layer and the surrounding air is chosen with their number, N_d, equal to that of the simulation charges either in the coating layer or in the surrounding air (figure 1). At these boundary points, pertinent boundary conditions have to be satisfied. These boundary conditions are expressed as follows:

(i) The potential, Φ, calculated at any point on the electrode surface is the algebraic sum of the potentials at this point produced by the simulation charges of the electrode and the surrounding air. Of course, the potential, Φ, must be equal to the applied voltage, i.e.

$$\Phi = V. \tag{2}$$

Instead of one boundary condition at each point on the electrode surface, two boundary conditions are satisfied at each point on the interface between the coating layer and surrounding air.

(ii) The potential, Φ_1, at any point on the interface is the algebraic sum of potentials at this point due to the simulation charges of the electrode and the surrounding air when the point is seen from the coating layer side. If the point is seen from the surrounding air side, the potential, Φ_2, is the algebraic sum of the potentials at this point due to the simulation charges of the electrode and the coating layer [6, 7, 15]. Of course, the potentials Φ_1 and Φ_2 should be equal (i.e. the potential is continuous), i.e.

$$\Phi_1 = \Phi_2 \qquad \text{or} \qquad \Phi_1 - \Phi_2 = 0. \tag{3}$$

(iii) The normal components of the field, E_{n1} and E_{n2}, at any point when seen from the coating layer and the surrounding air sides, respectively, are related to each other through the relative permittivity, ε_r, of the coating layer to satisfy the continuity of electric flux in the direction normal to the dielectric interface [6,7,15]. These field components are calculated using the same charges used in calculating the potentials Φ_1 and Φ_2, respectively.

$$\varepsilon_r E_{n1} - E_{n2} = 0. \tag{4}$$

Satisfaction of the boundary conditions using equations (2)–(4) applied at the respective boundary points results in a set of simultaneous equations (5) whose solution determines the unknown simulation charges.

$$\begin{bmatrix} P & 0 & P \\ 0 & P & -P \\ (\varepsilon_r - 1) f_n & -f_n & \varepsilon_r f_n \end{bmatrix} \begin{bmatrix} Q_1 \\ \cdots \\ Q_{N_e} \\ Q_{N_e+1} \\ \cdots \\ Q_{N_e+N_d} \\ Q_{N_e+N_d+1} \\ \cdots \\ Q_N \end{bmatrix} = \begin{bmatrix} V \\ \cdots \\ V \\ 0 \\ \cdots \\ 0 \\ 0 \\ \cdots \\ 0 \end{bmatrix}, \tag{5}$$

where P and f_n stand for the potential and normal field coefficients of a simulation charge calculated at a boundary point [6, 7, 15]. Once the simulation charges are known, the electric field and the potential can be calculated at any point in air and dielectric media for the investigated electrode system.

2.1.3. Determination of the electric potential and field. The potential, $\phi_1(r, z)$, and the radial and axial components, $E_{r1}(r, z)$ and $E_{z1}(r, z)$, at a point $p(r, z)$ located on the electrode surface or in the coating layer are expressed by equations (6*a*)–(6*c*). They are the sum of the potentials, the radial- and axial-field components produced at this point by the simulation charges (and their images) of the stressed electrode, and the air medium:

$$\phi_1(r, z) = \sum_{J=1}^{J=N_e} Q(J)P(J) + \sum_{J=N_e+N_d+1}^{J=N} Q(J)P(J), \tag{6a}$$

$$E_{r1}(r, z) = \sum_{J=1}^{J=N_e} Q(J)F_r(J) + \sum_{J=N_e+N_d+1}^{J=N} Q(J)F_r(J), \tag{6b}$$

$$E_{z1}(r, z) = \sum_{J=1}^{J=N_e} Q(J)F_z(J) + \sum_{J=N_e+N_d+1}^{J=N} Q(J)F_z(J). \tag{6c}$$

Here $P(J)$, $F_r(J)$ and $F_z(J)$ are, respectively, the potential and the radial- and axial-field coefficients calculated at the point $p(r, z)$ due to the Jth simulation charge and its image [15]. The coordinates of the Jth simulation charge and the coordinates of the point $p(r, z)$ determine these coefficients.

Similarly, the potential $\phi_2(r, z)$ and the radial and axial components, $E_{r2}(r, z)$ and $E_{z2}(r, z)$, at any point $p(r, z)$ in air medium are expressed by equations (7*a*)–(7*c*). They are the sum of the potentials and the radial- and axial-field components produced at this point by the simulation charges (and their images) of the stressed electrode and the dielectric coating medium:

$$\phi_2(r, z) = \sum_{J=1}^{J=N_e} Q(J)P(J) + \sum_{J=N_e+1}^{J=N_e+N_d} Q(J)P(J), \tag{7a}$$

$$E_{r2}(r, z) = \sum_{J=1}^{J=N_e} Q(J)F_r(J) + \sum_{J=N_e+1}^{J=N_e+N_d} Q(J)F_r(J), \tag{7b}$$

$$E_{z2}(r, z) = \sum_{J=1}^{J=N_e} Q(J)F_z(J) + \sum_{J=N_e+1}^{J=N_e+N_d} Q(J)F_z(J). \tag{7c}$$

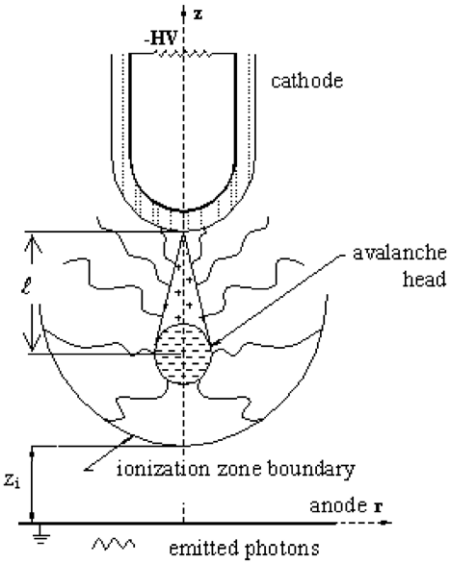

Figure 2. The development of the primary avalanche along the gap axis.

2.2. Criteria for the onset voltage of negative corona

When the electric field strength in the vicinity of the coated electrode surface reaches the value for inception of ionization of air molecules by electron collision, a primary avalanche starts to develop along the gap axis, where the field assumes maximum values, away from the coated electrode (figure 1). With the growth of the avalanche, more electrons are developed at its head, more photons are emitted in all directions and more positive ions are left in the avalanche's wake. The avalanche growth takes place under the combination of the field due to the applied voltage and the field of the positive ions in the wake of the avalanche itself. The growth of the avalanche continues as long as Townsend's first ionization coefficient, $\alpha(z)$, is greater than the electron attachment coefficient, $\eta(z)$, and terminates at $z = z_i$; i.e. at the ionization-zone boundary ($\alpha(z) = \eta(z)$) (figure 2), where the electrons get attached to the air molecules and form negative ions [7, 18].

For a successor avalanche to be started, the preceding avalanche should somehow provide an initiating electron at the stressed electrode surface, possibly by photoemission, positive ion impact, metastable action or field emission. Field emission is possible only at field strengths exceeding $5 \times 10^7\ \mathrm{V\,m^{-1}}$ [19]. Electron emission by positive-ion impact is more than two orders of magnitude less frequent than that by photoemission [6]. Metastables have been reported to have an effect approximately equal to that of positive ion impact [7]. Therefore, only the first mechanism (electron emission by photons) was considered in determining the onset voltage of a corona in the air gap.

For the successor avalanche to be started, the photons emitted from the primary avalanche that reach the cathode (the coated electrode) should act for the emission of a photo-electron, ($N_{\mathrm{eph}} = 1$). The condition for a new (successor) avalanche to develop [18] is

$$N_{\mathrm{eph}} = \gamma_{\mathrm{ph}} \int_{H-t}^{z_i} \alpha(\ell) g(\ell) \exp\left[\int_{H-t}^{z} \{\alpha(z) - \eta(z)\}\mathrm{d}z\right] \times \exp(-\mu\ell)\mathrm{d}\ell \geqslant 1, \quad (8)$$

where γ_{ph} is Townsend's second coefficient due to the action of photons, μ is the photon absorption coefficient, z_i is the distance measured along the gap axis determining the ionization-zone boundary (figure 2) and $g(\ell)$ is a geometric factor to account for the fact that some photons are not received by the cathode [18]. Field emission of electrons from the dielectric's surface takes place due to UV irradiation, under which dielectrics behave as metallic conductors [20]. Thus, equation (8) is valid in the presence or absence of the dielectric coating on the stressed electrode [7]. Equation (8) assumes the self-recurrence of the avalanche by developing its successor independent of the density of ions produced by radioactivity and cosmic rays in the surrounding atmosphere.

The onset voltage of a corona does not appear explicitly in relation (8). However, the applied voltage affects the values of α, η, etc. The onset voltage is the critical value that satisfies equality (8). It is calculated using the values available in [21] for the air parameters α, η, γ_{ph} and μ at atmospheric pressure, as given in the appendix.

3. Experimental procedures

The experiments were carried out in atmospheric air with bare and dielectric-coated rod–plane electrode systems. Cylindrical hemispherically-capped rods of radii 3 and 4 mm and having a length of 0.25 m were tested. The rods were coated with an insulating varnish of thickness t equal to 0.5 and 0.375 mm. The lower plate electrode was of 0.15 m in diameter with a rounded edge to avoid the occurrence of coronas at this edge. The varnish used was Dolphen BC-352 clear epoxy varnish. Its relative permittivity is $\varepsilon_r = 3.29$. The gap spacing, H, in the experiments was varied within a range of 0.04 to 0.10 m for all rod–plane gaps. A high-voltage dc source (Hipotronics, Model 800PL-10MA series) was used to energize the stressed electrode up to 80 kV and 10 mA. The overall accuracy of voltage measurement was considered to be within ±2%. The stressed electrode was connected to the HV source through a water resistance of 1 MΩ as a current-limiting resistor.

The audible onset voltage of the corona was measured on the surface of the bare and dielectric-coated rod electrodes. The applied voltage was raised to about 90% of the expected value at a rate of $1\ \mathrm{kV\,s^{-1}}$ and thereafter at a rate of about $0.1\ \mathrm{kV\,s^{-1}}$ until human ears could just hear the audible flutter sound in the dark, quiet, closed laboratory [22]. The time interval between two successive applied voltages was at least 1 min. At least ten measurements were taken to estimate the mean of each measuring point. The relative standard deviation of the mean values was generally smaller than 1%. The tests were conducted in dry air at room temperature (about 22–25 °C) and atmospheric pressure.

4. Results and discussion

To check the accuracy of the charge simulation, check points were selected midway between the boundary points on the stressed electrode and dielectric surface (figure 1). The potential and the deviation angle of the field at the stressed electrode surface were assessed at the check points to check how well the Dirichlet condition is satisfied at the stressed electrode surface. Also, to check how well the Neumann

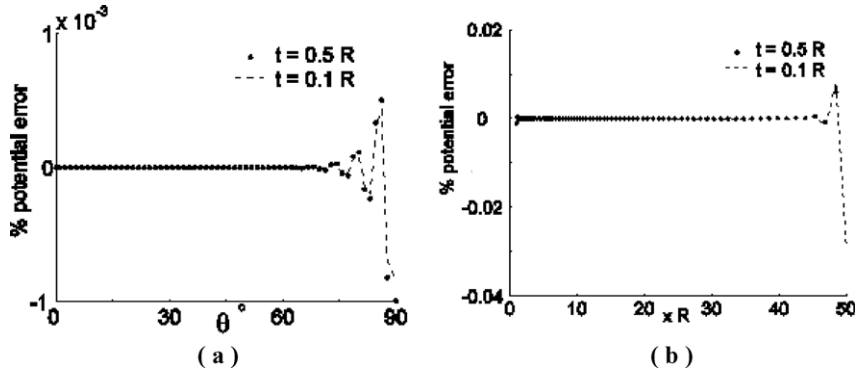

Figure 3. The variation of percentage potential errors at the surface of the stressed electrode at $G = 10$ and $\varepsilon_r = 3$ versus: (*a*) the angular location, θ, on the hemispherical part, and (*b*) along the cylindrical part.

condition is satisfied at the dielectric surface, the continuity of the electric potential, the equality of tangential components of the field and the normal electric field error at the dielectric surface, was also assessed at the check points. This check of accuracy was made for a wide range of coating thickness, t (0.075–1.0 times rod radius, R), and gap factor, G, defined as $G = H/R$, (G = 1–200). The accuracy remained the same for these investigated ranges.

The accuracy of a simulation depends strongly on the assumptions involved in the choice of the number and coordinates of the simulation charges. The number of charges was found to be $n_e = n_d = n_a = 30$, $m_e = 80$, k = integral part of (R/t) for $t \leqslant 0.5R$ and $k = 2$ for $t \geqslant 0.5R$ and $m_d = m_a = km_e$. The value of k increased from 2 to 13 from the considered thick coatings to the thin coatings, respectively. Therefore, the best accuracy is achieved when $N_e = 111$; $N_d = n_d + m_d$ increases from 190 to 1070. So, the total number of simulation charges $N = N_e + N_d + N_a$ increases from 491 to 2251 charges, from the considered thick coatings to the thin coatings, respectively. The simulation accuracy was found to be highly influenced by the variables f_0, f_1, f_2 and δt. An acceptable accuracy is achieved in the investigated ranges of dielectric thickness, t, and gap factor, G, when these factors take values of 0.9, 0.18, 1.03 and 0.9 times the coating thickness t, respectively. The accuracy results given below are samples computed with gap factor $G = 10$, coating relative permittivity $\varepsilon_r = 3$, coating thickness $t = 0.1$ and $t = 0.5$ times the rod radius, R.

At the surface of the stressed electrode, the percentage errors of the potential and the electric field deviation angle are calculated along the spherical part and over a length of 50 times the rod radius, R, of the cylindrical part. Figure 3 shows the percentage errors of the simulated potential. The maximum percentage error does not exceed 0.001% and 0.03% along the hemispherical and the cylindrical parts, respectively. Potential errors on the electrode surface of less than 0.1% are considered reasonable for accurate field solution [15]. The electric field deviation angle at the surface of the stressed electrode does not exceed 0.15° and 0.25° along the hemispherical and the cylindrical parts, respectively. Using optimization techniques for bare rod–plane gaps [23], bare needle–plane gaps [24] and bare point–cup gaps [25], maximum deviation angles of 4.2°, 0.9° and 0.39° are observed on the stressed electrode, respectively. This demonstrates the enhanced accuracy and effectiveness of the present method.

At the dielectric surface, the continuity of the electric potential, the equality of tangential components of the field and the continuity of the normal electric field errors are computed along the spherical part and over a length of 25 times the rod radius, R, of the cylindrical part. This conforms to the fact that the simulation accuracy is less on the dielectric surface when compared with that along the rod itself. The maximum percentage error for the continuity of the electric potential is less than 0.002% along both the hemispherical and the cylindrical parts. Also, the percentage errors for the equality of the tangential components of the field are less than 3% and 6% along the hemispherical and the cylindrical parts, respectively. Figure 4 shows the percentage errors for the normal electric field; the maximum percentage error does not exceed 1.5% and 1% along the hemispherical and the cylindrical parts, respectively.

Figure 5 shows the per-unit potential distribution along the gap axis starting from the stressed electrode surface. It is quite clear that the potential decreases continuously along the gap axis without showing a discontinuity at the interface between the coating layer and the surrounding air.

Figure 6 shows the field distribution along the gap axis starting from the electrode surface for a unit voltage applied to the coated electrode at $R = 10$ mm, $t = 5$ mm, $H = 0.1$ m and $\varepsilon_r = 3$. It is quite clear that the field shows a discontinuity at the interface where the ratio $E_{air}/E_{coating\ layer}$ is equal to the relative permittivity, $\varepsilon_r (= 3)$, of the coating layer. For comparison purposes, figure 6 shows also the field distribution for a bare electrode of the same radius ($R = 10$ mm) calculated using the method described in [26]. It appears that the coated layer suppresses the field in the vicinity of the electrode surface in comparison with the bare one. This reflects itself as an increase in the voltage of onset of a corona at the surface of coated electrodes. Also, figure 6 shows the field distribution for a bare electrode of radius equal to the overall radius ($=R + t = 15$ mm) of the coated electrode; the maximum value of the field on its surface is greater than that value on the coated electrode surface.

Figure 7 depicts the effect of coating layer thickness, t, on the value of the maximum electrical field, E_{max}, at different values of the relative permittivity, ε_r. It decreases with decreasing relative permittivity of the coating, ε_r. Also, it increases on the coating surface with decreasing coating thickness, reaching the ordinate axis at zero thickness value,

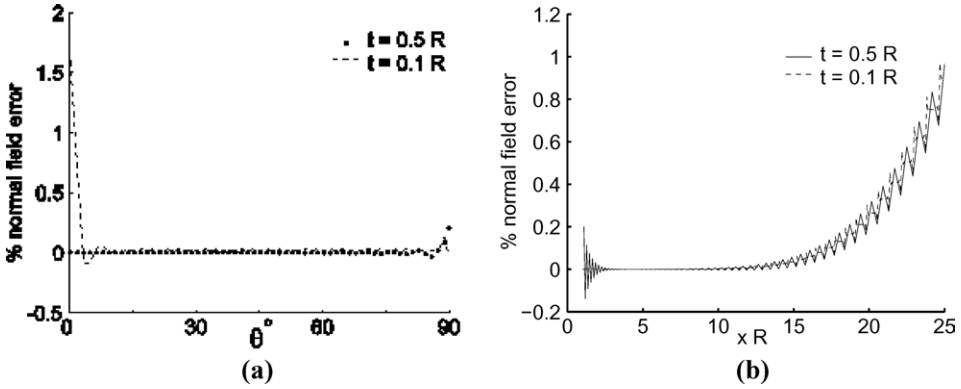

Figure 4. The variation of the normal field error at the dielectric surface at $G = 10$ and $\varepsilon_r = 3$ versus: (a) the angular location, θ, on the hemispherical part, and (b) along the cylindrical part.

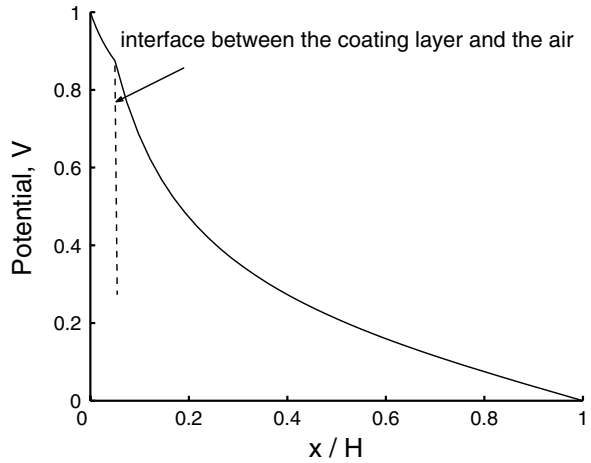

Figure 5. The potential distribution along the gap axis for a coated electrode stressed by a unit voltage at $R = 1$, $t = 0.5$, $H = 10$ and $\varepsilon_r = 3$.

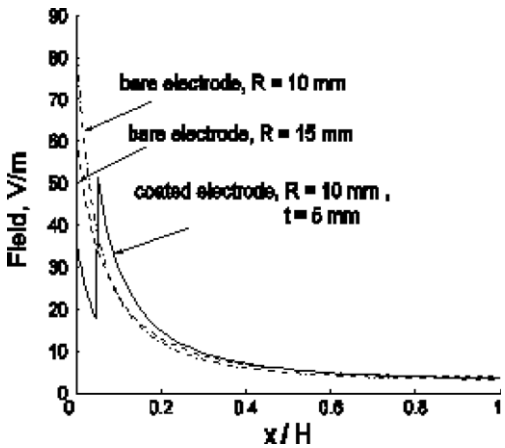

Figure 6. Electric field distribution along the gap axis, where the bare and coated electrodes are stressed by a unit voltage. For coated electrodes: $R = 10$ mm, $t = 5$ mm, $\varepsilon_r = 3$. For bare electrodes: $R = 10$ and 15 mm.

which agrees with the E_{max} value calculated earlier [26] for a bare rod. Also, figure 8 depicts the effect of ε_r, at different values of coating thickness, t, on the value of E_{max}. It decreases on the coating surface slightly with decreasing ε_r at different values of t. As ε_r decreases, the curves intersect the ordinate

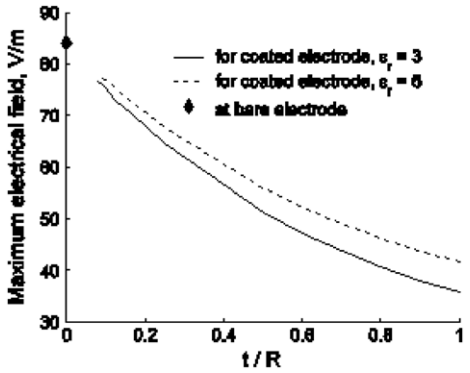

Figure 7. Effect of coating layer thickness on the maximum electrical field for different values of relative permittivity (ε_r) at $R = 10$ mm and $H = 0.1$ m.

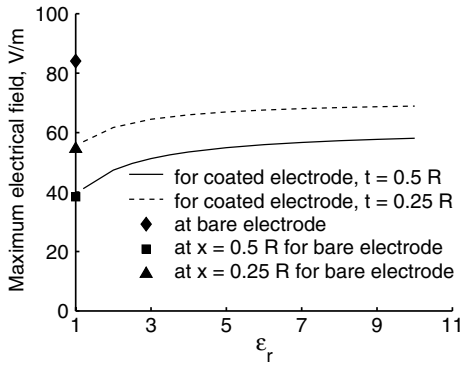

Figure 8. Effect of relative permittivity of coating material (ε_r) on the maximum electrical field at $R = 10$ mm, $H = 0.1$ m, $t = 0.5R$ and $t = 0.25R$.

axis when ε_r equals unity. The point of intersection is the field value calculated for a bare electrode [26] at a distance equal to the thickness of the coating layer considered for coated electrodes at $\varepsilon_r = 1$.

It is quite clear from figures 6–8 that the dielectric coating is more effective in suppressing the field (i.e. increasing the onset voltage of the corona) on the electrode surface. This ensures an important general design feature of the coated insulation system [27, 28]: to maximize the onset voltage on a coating surface, a thick coating with a low relative permittivity of the available coating material is used.

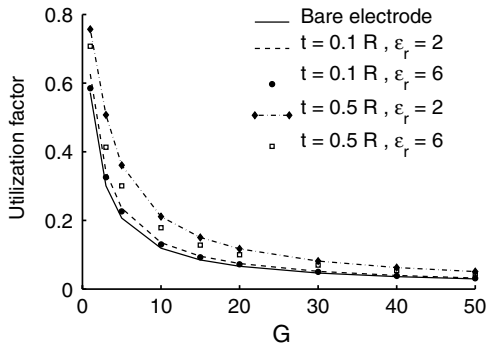

Figure 9. Effect of gap factor, G, on the the utilization factors for bare and coated electrodes; the coating material has different values of thickness, t, and relative permittivities, ε_r.

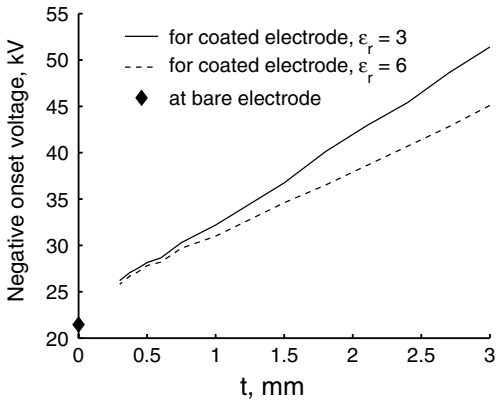

Figure 10. Effect of coating layer thickness, t, on the negative onset voltage of a corona at different values of permittivity of the coating layer: $R = 3$ mm and $H = 0.1$ m.

In a nonuniform field gap, if the average field in the gap, $E_{av}(=V/H)$, is greater than 0.2 times the maximum field, E_{max}, the corona phenomena will be similar to those in a uniform field, i.e. breakdown will occur without any preceding corona [6]. In coated electrode–plane gaps, E_{max} is the maximum electrical field value at the coating surface.

The utilization factor, U, which is defined as $U = E_{av}/E_{max}$, is computed for various values of G, at different values of coating thickness and relative permittivities. The computed utilization factor for coated and bare rod–plane gaps is plotted in figure 9; this factor is larger for coated electrodes. Also, for coating electrodes, this factor is larger in the case of smaller coating permittivity and larger coating thickness values. As the present work is about the onset voltage of a corona, U is chosen to be less than 0.2; i.e. G is roughly $\geqslant 10$, figure 9.

Figure 10 shows the increase of the calculated onset voltage values with increasing thickness of the coating layer, t, at different values of ε_r. The onset voltage values at a smaller value of ε_r are higher than those for the larger one. This is simply explained by considering the low electrical field values near the coating with a lower value of ε_r for the same applied voltage. The extension of the curves intersects the ordinate axis at the calculated value for the bare electrode, i.e. at zero thickness of the coating layer.

Figures 11 and 12 show the increase of the calculated and measured onset voltage values with increasing height of gap

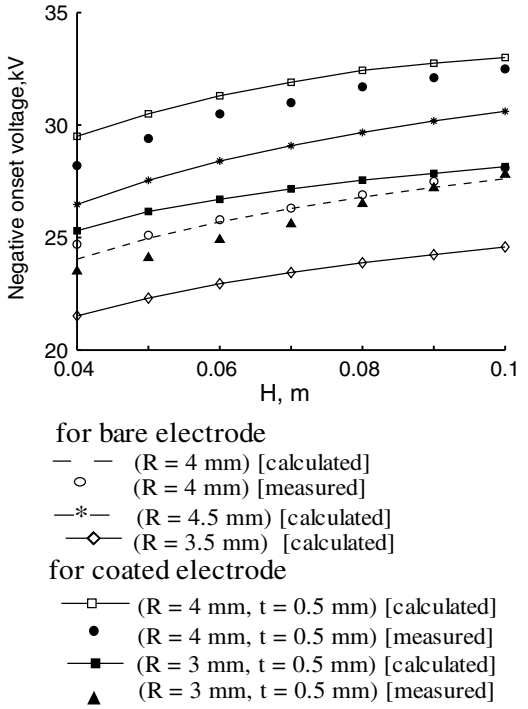

Figure 11. Measured and calculated negative onset voltages of corona versus the gap spacing, H, for bare and coated electrodes at different rod radii, R, and at the same coating thickness, t.

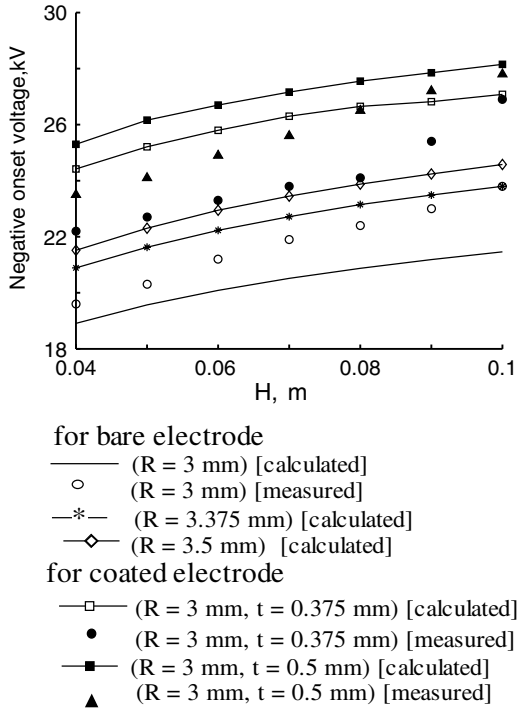

Figure 12. Measured and calculated negative onset voltage of corona versus the gap spacing, H, for bare and coated electrodes at the same rod radius, R, and at different coating thickness, t.

spacing, H, for bare and coated electrodes. The onset voltage values for the thick bare and coated electrodes are higher than those for the thin ones. This is simply explained by considering the low electrical field values near the thicker electrodes for

the same applied voltage. The calculated onset voltage values agreed with those measured experimentally within 10%. Some of the uncertainties in the results could be due to the fact that the corona onset voltage may depend on the voltage rise time because of positive charge accumulation on the dielectric before corona inception. Figure 11 shows the calculated onset voltage values for bare electrodes having overall radii of $R + t = 3.5$ and 4.5 mm of the coated electrode. The onset voltage values are less than the corresponding values on the coated electrode surface of radius R and coating thickness t. This means that dielectric coating is more effective in increasing the onset voltage of a corona on the electrode surface than is increasing the same electrode radius. Also, figure 12 shows that the onset voltage of a corona on thick-coated electrodes is higher than the corresponding value on thin-coated electrodes. From figures 10–12, it is seen that the insulation performance of air-gaps is improved by using coated electrodes.

5. Conclusions

1. The electrical field values in dielectric-coated hemispherically-capped rod–plane gaps are calculated using the charge simulation technique at a wide range of gap factor and dielectric coating thickness values. The number of simulation charges in both the air and the dielectric coating has to increase tremendously with the decrease of the thickness of dielectric layer in order to satisfy the Dirichlet condition at the stressed rod and the Neumann condition at the dielectric surface. The coated layer reduces the field in the vicinity of the coated hemispherically-capped rod surface in comparison with the bare one.
2. The maximum electrical field value, $E_{\max}$, on the coating surface decreases with increasing coating thickness and decreasing relative permittivity, ε_r, of the coating material. Hence, to maximize the onset voltage on the coating surface, a thick coating of the available coating material with a low relative permittivity is suggested.
3. The computed utilization factor for coated rod–plane gaps is larger than that of a bare rod–plane gap having the same dimensions. Also, in the case of coated rod–plane gaps, this factor is larger in the case of a smaller value of permittivity and a larger value of coating thickness of the available coating material.
4. The onset voltage values for the thick bare and coated electrodes are higher than those for the thin ones. This is simply explained by considering the low electrical field values near the thicker electrodes for the same applied voltage.
5. The calculated onset voltages agreed satisfactorily with those measured experimentally, within 10%.

Appendix. Physical parameters [21]

To evaluate the corona onset voltages in air, the physical parameters involved in the calculation of the avalanche growth are required. The values used for α, η, γ_{ph} and μ are as follows when the electric field, E, is in kV cm^{-1}.

Ionization coefficient, α:

$$\begin{aligned}
\alpha\ (\mathrm{cm}^{-1}) &= 3631.736\mathrm{e}^{-167.96/E} && 19.0 \leqslant E \leqslant 45.6,\\
\alpha\ (\mathrm{cm}^{-1}) &= 7358.32\mathrm{e}^{-200.792/E} && 45.6 < E \leqslant 182.4,\\
\alpha\ (\mathrm{cm}^{-1}) &= 114\,24.77\mathrm{e}^{-278.003/E} && 182.4 < E \leqslant 608.0.
\end{aligned} \tag{A.1}$$

Attachment coefficient, η:

$$\eta\ (\mathrm{cm}^{-1}) = 9.8648 - 0.541E + 0.011\,4474E^2. \tag{A.2}$$

Absorption coefficient, μ:

$$\mu\ (\mathrm{cm}^{-1}) = 5. \tag{A.3}$$

Townsend's second coefficient, γ_{ph}:

Townsend's second coefficient, γ_{ph}, due to the action of photons is considered constant at its value in atmospheric pressure, $\gamma_{ph} = 0.003$.

References

[1] Arrillaga J 1998 *High Voltage Direct Current Transmission (IEE Power Engineering Series)* (London: IEE)

[2] Nayak S K and Thomas M J 2005 An integro-differential equation technique for the computation of radiated EMI due to corona on HV power transmission lines *IEEE Trans. Power Delivery* **20** 488–93

[3] ACGIH 1992 Threshold limit values for chemical substances and physical agents and biological exposure indices (Cincinnati, OH: ACGIH) http://www.acgih.org

[4] Griffin G D, Kurka K, Nolan M G, Morris M D, Sauers I and Votaw P C 1989 Cytotoxic activity of diulfur decafluoride (S_2F_{10}), a decomposition product of electrically-stressed SF_6 *In Vitro* **25** 673–5

[5] Yamazaki K and Olsen R G 2004 Application of a corona onset criterion to calculation of corona onset voltage of stranded conductors *IEEE Trans. Dielectrics Electr. Insul.* **11** 674–80

[6] Abdel-Salam M, Anis H, El-Morshedy A and Radwan R 2000 *High Voltage Engineering-Theory and Practice* 2nd edn (New York: Dekker) pp 149–84

[7] Abdel-Salam M, Turky A and Hashem A 1998 The onset voltage of coronas on bare and coated conductors *J. Phys. D: Appl. Phys.* **31** 2550–6

[8] Ming L, Fromm U, Leijon M, Windmar D, Walfridon L and Vlastos A 1997 Insulation performance of covered rod/plane air-gap under lightning impulse voltage *10th Int. Symp. on High Voltage Engineering (Montreal, Quebec, Canada, 25–29 August 1997)*

[9] Blennow H J M, Sjoberg M L A, Leijon M A S and Gubanski S M 2000 Electric field reduction due to charge accumulation in a dielectric-covered electrode system *IEEE Trans. Dielectrics Electr. Insul.* **7** 340–5

[10] Sjoberg M L A 2003 Charge accumulation in hybrid high voltage insulation *PhD Thesis* Chalmers University of Technology, School of Electrical and Computer Engineering, Gotenberg, Sweeden

[11] Weeks W 1981 *Transmission and Distribution of Electrical Energy* (New York: Harper and Row)

[12] Morcos M M, Zhang S, Srivastava K D and Gubanski S M 2000 Dynamics of metallic particle contaminants in GIS with dielectric coated electrodes *IEEE Trans. Power Delivery* **15** 455–60

[13] Morcos M M, Zhang S and Srivastava K D and Gubanski S M 2002 Management of particle contamination in GIS/GITL by electrode coating (Paris: Cigre) no. 15-401

[14] Wadhwa C L 2002 *Electrical Power Systems* (New Delhi: New Age International)

[15] Malik N H 1989 A review of the charge simulation method and its applications *IEEE Trans. Electr. Insul.* **24** 3–14
[16] Malik N H and Qureshi A H 1979 Calculation of discharge inception voltages in SF_6-N_2 mixtures *IEEE Trans. Electr. Insul.* **14** 70–76
[17] Inuishi Y 1981 Electrical discharges of SF_6 gas in nonuniform fields *Electra* **84** 45–52
[18] Abdel-Salam M 1976 Calculating the effect of high temperature on the onset voltages of negative discharges *J. Phys. D: Appl. Phys.* **9** L149–54
[19] Novak J P and Bartnikas R 2000 Effect of dielectric surfaces on the nature of partial discharges *IEEE Trans. Electr. Insul.* **7** 146–51
[20] Gosho Y and Saeki M 1987 Secondary electron emission from dielectric surface under atmospheric air conditions due to UV irradiation *5th Int. Symp. on High Voltage Engineering (Braunschweig, Germany)* paper 23.24
[21] Abdel-Salam M and Stanek E K 1988 On the calculation of breakdown voltages for uniform electric fields in compressed air and SF_6 *IEEE Trans. Indust. Appl.* **24** 1025–30
[22] Arora R and Halder P 2001 Investigation of the inception of streamer corona in SF_6 gas *12th Int. Symp. on High Voltage Engineering* vol 2 *(Bangalore, India, 20–24 August 2001)*
[23] Iravani M R and Raghuveer M R 1982 Accurate field solution in the entire interelectrode space of a rod–plane gap using optimized charge simulation *IEEE Trans. Electr. Insul.* **17** 333–7
[24] Abouelsaad M M and El-Bahy M M 2000 Accurate field computation of needle–plane gaps using an optimized charge simulation method *2000 IEEE Conf. on Electrical Insulation and Dielectric Phenomena (Canada, 15–18 October 2000)*
[25] El-Bahy M M 2002 Onset voltage of negative corona in point-cup gaps *37th International Universities Power Engineering Conference (UPEC) (Staffordshire University, UK, 9–11 September 2002)* pp 549–53
[26] Abou Seada M S and Nasser E 1968 Digital computer calculation of the electric potential and field of a rod gap *IEEE Proc.* **56** 813–20
[27] Blennow H J M, Serdyuk Yu V, Leijon M A S and Gubanski S M 2002 Active high voltage insulation *J. Electrostatics* **55** 159–72
[28] El-Bahy M M 2005 A numerical modelling of microdischarge threshold in uniform electric fields *J. Phys. D: Appl. Phys.* **38** 103–12